Acta Cryst. (1976). B32, 572

Charge Density Studies below Liquid Nitrogen Temperature: X-ray Analysis of *p*-Nitropyridine *N*-Oxide at 30 K

BY Y. WANG,† R. H. BLESSING,‡ F. K. ROSS§ AND P. COPPENS*

Chemistry Department, State University of New York at Buffalo, Buffalo, New York 14214, *U.S.A.*

(*Received* 10 *February* 1975; *accepted* 24 *June* 1975)

The structure of *p*-nitropyridine *N*-oxide has been redetermined at both 30 and 300K. Data were collected in a step-scan mode and intensities obtained through profile-analysis. The *b* axis, which is normal to the molecular planes, contracts considerably on cooling, and thermal parameters decrease by a factor of about six, in agreement with predictions based on a simple harmonic model. The orientation of the thermal ellipsoids is essentially the same at both temperatures. Comparison of bond lengths at the two temperatures clearly demonstrates the necessity of a bond-length correction for shortening due to thermal motion. Bond lengths agree well after correction according to a rigid-body model. Difference densities were calculated with positional parameters and hydrogen thermal parameters from an independent low-temperature neutron study. Densities calculated with data cut-offs of $\sin\theta/\lambda = 0{\cdot}65$, 0·75, and 1 Å^{-1} indicate an appreciable increase in noise level on inclusion of high-order reflections. The height of the lone-pair density increases with data cut-off while the densities in the bond regions are much less affected, thus confirming the hypothesis that the lone-pair electrons contribute to high-order scattering. Similarly, difference maps based on a high order X-ray refinement ($\sin\theta/\lambda > 0{\cdot}75$ Å^{-1}) underestimated the density in the lone-pair regions.

Introduction

Several earlier charge density studies of molecular crystals have clearly indicated the desirability of performing the necessary diffraction experiments at reduced temperatures (Verschoor & Keulen, 1971; Coppens & Vos, 1971; Coppens, 1974). Though the effect of thermal averaging on the density is becoming better understood in a quantitative sense (Coulson & Thomas, 1971; Ruysink & Vos, 1974; Coppens, 1975), reduction of the thermal smearing of the rest density and the corresponding increase in thermal resolution remain of considerable importance. Of particular interest is the measurable intensity of high-order reflections at low temperature, and the corresponding possibility of calculating difference densities based on parameters from a high-order X-ray refinement. A parallel neutron-diffraction study would not be necessary, if the high-order intensities were truly independent of the charge density rearrangement upon molecule formation.

Equipment for single-crystal diffraction studies down to liquid-helium temperatures has been developed and applied in a series of structure determinations (Coppens, Ross, Blessing, Cooper, Larsen, Leipoldt, Rees & Leonard, 1974). This report describes its first application to charge density determination by diffraction methods.

The molecule of *p*-nitropyridine *N*-oxide was selected because of its relatively simple orthorhombic structure (Eichhorn, 1956), the chemically interesting polar N–O bond, which is formulated as $N \rightarrow O$ in the lowest valence bond resonance structure, and the presence of low-frequency molecular motions, which lead to large thermal parameters at room temperature.

The study consists of both a room-temperature (300 K) and a low-temperature (30 K) X-ray study. A parallel series of neutron measurements at 30 K has not yet yielded reliable thermal parameters (Ross & Williams, 1973), owing to difficulties with the neutron diffraction liquid-helium equipment.‖ In the present study the neutron *positional* parameters are compared with X-ray results and used in the calculation of difference density maps.

Experimental

Crystals were grown as described by Eichhorn (1956). Data were collected on an automated Picker four-circle diffractometer with Mo $K\alpha$ radiation. The X-ray cryostat allows a temperature stability of 0·1°. The data set was collected on a capillary-enclosed crystal of 0·25 mm average diameter. The internal consistency indices between symmetry-related reflections (analogous to the agreement indices between observed and calculated structure factors) are, for the liquid helium data, $R(F^2) = 2{\cdot}5\%$ [1·1% for the 665 strongest reflections with $F^2/\sigma(F^2) > 50$], and, for the room tem-

* Author to whom correspondence should be addressed.

† Present address: Division of Chemistry, National Research Council of Canada, Ottawa, Canada.

‡ Present address: Department of Chemistry, Mercyhurst College, Erie, Pennsylvania, U.S.A.

§ Present address: Department of Chemistry, Virginia Polytechnic Institute, Blacksburg, Virginia, U.S.A.

‖ *Note added in proof:*– A low-temperature neutron diffraction study has now been completed and is desribed in an article to be submitted to *Acta Cryst.* (P. Coppens & M. S. Lehmann).

perature data, 4·0% [1·7% for the 226 strongest reflections with $F^2/\sigma(F^2)>50$]. For each reflection the full profile of a θ–2θ step scan was recorded and analyzed with a procedure described elsewhere (Blessing, Coppens & Becker, 1974). The two symmetry-related data sets were averaged after application of Lorentz–polarization and absorption corrections. The largest contraction on cooling is observed in the b axis direction, which corresponds to the normal to the molecular planes (see Table 1).

Table 1. *Crystal data*

Space group $Pnma$ (C_{2h}^{16}); $Z=4$; $\mu=1{\cdot}489$ cm^{-1} (Mo $K\alpha$ radiation $\lambda=0{\cdot}71069$ Å)

	298 K (X-ray)	160 K (X-ray)	30 K (X-ray)
a	12·530 (5)	12·517	12·498 (6)
b	6·010 (2)	5·914	5·814 (2)
c	7·899 (4)	7·875	7·824 (2)
V (Å^3)	594·84	582·95	568·52
d_x	1·564	1·596	1·637
$(\sin\theta/\lambda)_{max}$	0·76	—	1·0
Number of unique reflections	1162	—	2201

Refinement

X-ray data

The function minimized in the refinements of both sets of X-ray data is $\sum w(F_o^2-kF_c^2)$ in which the weight w is defined by $\sigma^2=1/w=\sigma^2(\text{counting})+(0{\cdot}02F_o^2)^2$. Scattering factors used are as published in *International Tables for X-ray Crystallography* for C, N and O and as given by Stewart, Davidson & Simpson for H (1965). A separate high-order refinement ($\sin\theta/\lambda>0{\cdot}75$ Å^{-1}) was performed on the low-temperature data set. Positional and thermal parameters and final agreement indices are listed in Tables 2 and 3.* It is of interest to note that the estimated standard deviations are lower by a factor 2–3 at 30 K.

* A list of structure factors has been deposited with the British Library Lending Division as Supplementary Publication No. SUP 31231 (14 pp., 1 microfiche). Copies may be obtained through The Executive Secretary, International Union of Crystallography, 13 White Friars, Chester CH1 1NZ, England.

Table 2. *Atomic fractional coordinates* ($\times 10^4$) *and thermal parameters* (Å$^2\times 10^4$)

The temperature factor is of the form

$$\exp\left[-2\pi^2(U_{11}a^{*2}h^2+U_{22}b^{*2}k^2+U_{33}c^{*2}l^2-2U_{13}a^*c^*hl)\right].$$

		298 K (X-ray)	30 K (X-ray)	30 K (X-ray $\sin\theta/\lambda>0{\cdot}75$)	30 K (neutron) (Ross & Williams, 1973)
O(1)	x	1360 (1)	1308 (1)	1310 (1)	1308 (5)
	z	8068 (2)	8064 (1)	8061 (1)	8055 (9)
O(2)	x	3872 (2)	3881 (1)	3881 (1)	3881 (5)
	z	1359 (2)	1331 (1)	1334 (1)	1347 (8)
O(3)	x	5166 (1)	5179 (1)	5177 (1)	5172 (5)
	z	3156 (2)	3183 (1)	3181 (1)	3186 (8)
N(4)	x	2030 (1)	1993 (1)	1992 (1)	1991 (3)
	z	6815 (3)	6819 (1)	6820 (1)	6821 (5)
N(5)	x	4213 (2)	4220 (1)	4223 (1)	4224 (3)
	z	2812 (2)	2815 (1)	2811 (1)	2811 (5)
C(6)	x	3096 (2)	3065 (1)	3064 (1)	3062 (4)
	z	7137 (3)	7172 (1)	7172 (1)	7173 (7)
C(7)	x	3823 (2)	3813 (1)	3814 (1)	3815 (4)
	z	5855 (3)	5879 (1)	5881 (1)	5880 (7)
C(8)	x	3457 (2)	3448 (1)	3449 (1)	3450 (4)
	z	4208 (3)	4206 (1)	4205 (1)	4205 (7)
C(9)	x	2374 (2)	2364 (1)	2364 (1)	2363 (4)
	z	3872 (3)	3831 (1)	3829 (1)	3826 (7)
C(10)	x	1678 (2)	1644 (1)	1640 (1)	1642 (4)
	z	5181 (3)	5162 (1)	5165 (1)	5159 (7)
H(C6)	x	3272 (16)	3226 (13)		3266 (8)
	z	8232 (26)	8364 (19)		8521 (14)
H(C7)	x	4564 (20)	4600 (13)		4655 (9)
	z	6122 (28)	6172 (19)		6184 (16)
H(C8)	x	2170 (19)	2117 (12)		2066 (9)
	z	2759 (30)	2657 (19)		2531 (13)
H(C10)	x	918 (17)	894 (12)		769 (9)
	z	5055 (24)	4999 (18)		4979 (16)

		298 K	30 K	30 K (high-order)
O(1)	U_{11}	494 (10)	70 (4)	65 (5)
	U_{22}	657 (13)	114 (3)	111 (3)
	U_{33}	581 (11)	82 (3)	82 (2)
	U_{13}	242 (10)	48 (2)	35 (2)
O(2)	U_{11}	706 (13)	107 (4)	97 (5)
	U_{22}	764 (14)	112 (3)	120 (3)
	U_{33}	357 (10)	52 (2)	57 (2)
	U_{13}	32 (9)	−10 (3)	−4 (2)
O(3)	U_{11}	326 (9)	39 (3)	51 (5)
	U_{22}	1048 (16)	151 (3)	152 (3)
	U_{33}	680 (13)	109 (3)	96 (3)
	U_{13}	126 (9)	0 (3)	9 (2)
N(4)	U_{11}	325 (10)	55 (4)	43 (4)
	U_{22}	413 (13)	64 (3)	72 (3)
	U_{33}	466 (13)	63 (3)	65 (2)
	U_{13}	93 (10)	14 (3)	13 (2)
N(5)	U_{11}	426 (12)	61 (4)	55 (5)
	U_{22}	480 (13)	70 (3)	75 (3)
	U_{33}	424 (13)	68 (3)	61 (2)
	U_{13}	56 (11)	8 (3)	7 (2)
C(6)	U_{11}	378 (13)	54 (4)	62 (5)
	U_{22}	456 (16)	82 (3)	85 (3)
	U_{33}	317 (13)	58 (3)	59 (3)
	U_{13}	−37 (12)	−11 (3)	−2 (2)
C(7)	U_{11}	269 (11)	52 (4)	52 (5)
	U_{22}	436 (15)	79 (3)	88 (3)
	U_{33}	387 (13)	62 (3)	58 (3)
	U_{13}	−60 (10)	−9 (3)	−5 (2)
C(8)	U_{11}	282 (11)	52 (4)	56 (5)
	U_{22}	362 (14)	71 (3)	74 (3)
	U_{33}	335 (11)	58 (3)	56 (3)
	U_{13}	39 (11)	15 (3)	6 (2)
C(9)	U_{11}	355 (12)	56 (4)	47 (5)
	U_{22}	414 (15)	75 (4)	80 (3)
	U_{33}	358 (14)	62 (3)	67 (3)
	U_{13}	−63 (11)	−5 (3)	−2 (2)
C(10)	U_{11}	268 (12)	50 (4)	56 (5)
	U_{22}	458 (17)	85 (4)	86 (3)
	U_{33}	530 (15)	73 (3)	70 (3)
	U_{13}	−34 (12)	−8 (3)	2 (2)
H(C6)	U	291 (55)	63 (35)	
H(C7)	U	531 (72)	70 (39)	
H(C9)	U	489 (72)	119 (39)	
H(C10)	U	433 (65)	71 (36)	

Table 2 (*cont.*)

		30 K (neutron) (Ross & Williams, 1973)
H(C6)	U_{11}	208 (21)
	U_{22}	300 (30)
	U_{33}	204 (26)
	U_{13}	−12 (8)
H(C7)	U_{11}	156 (22)
	U_{22}	511 (42)
	U_{33}	192 (30)
	U_{13}	−9 (10)
H(C9)	U_{11}	269 (25)
	U_{22}	408 (34)
	U_{33}	73 (24)
	U_{13}	−67 (16)
H(C10)	U_{11}	123 (18)
	U_{22}	374 (37)
	U_{33}	297 (30)
	U_{13}	−22 (22)

Table 3. *Agreement indices of least-squares refinement*

	298 K	30 K
k (scale factor)	3·287 (10)	4·032 (8)
g (isotropic extinction coefficient)	$0{\cdot}065\times10^{-4}$	$0{\cdot}11\times10^{-4}$
N_o [number of reflections with $F_o^2\geq3\sigma(F_o^2)$]	512	1422
N (number of variables)	74	74
$S=[\sum w(F_o-F_c)^2/N_o-N_v]^{1/2}$	1·623	1·916
$R=(\sum\|F_o-F_c\|^2/\sum F_o^2)^{1/2}$	0·035	0·036
$Rw=(\sum w\|F_o-F_c\|^2/\sum wF_o^2)^{1/2}$	0·032	0·038
$R(F^2)=[\sum\|F_o^2-F_c^2\|/\sum F_o^2]^{1/2}$	0·033	0·053
$Rw(F^2)=[\sum w\|F_o^2-F_c^2\|/\sum wF_o^2]^{1/2}$	0·063	0·076

Molecular structure and asphericity shifts

As found earlier by Eichhorn (1956), the molecules are planar and located in the mirror planes at $y=\frac{1}{4}$ and $y=\frac{3}{4}$. The correction for apparent bond shortening due to thermal vibrations, applied on the basis of the rigid-body TLS analysis (Schomaker & Trueblood, 1968), is very small at 30 K, but appreciable at room temperature (Table 4). The agreement between the two sets of results is satisfactory except for the C(6)–C(7) and C(9)–C(10) bonds (see Fig. 1 for numbering of atoms) which appear either undercorrected or systematically shortened at room temperature. Nevertheless, the comparison clearly demonstrates the

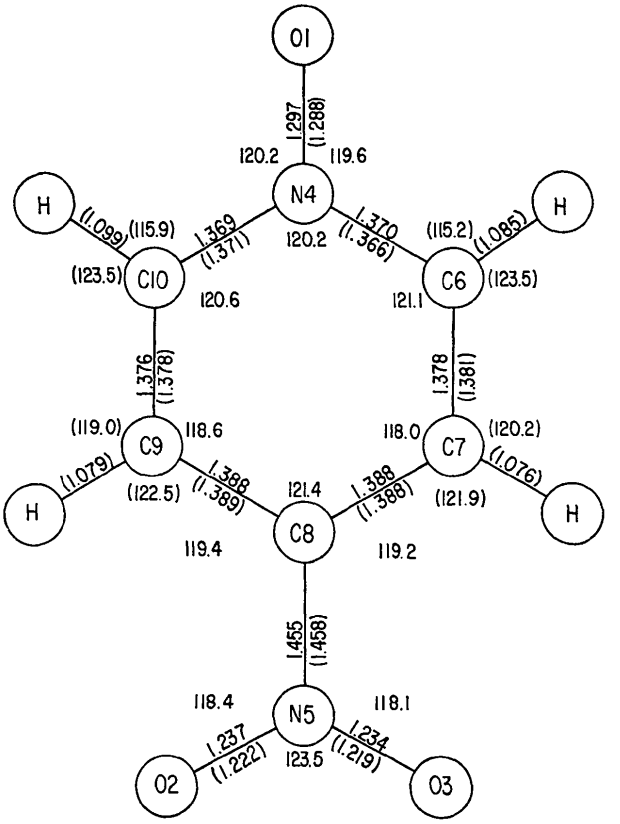

Fig. 1. Atom numbering, and bond lengths and angles at 30 K (*cf.* Table 4). Bond lengths and angles from the neutron diffraction study are given in parentheses.

Table 4. *Bond lengths*

	30 K X-ray		30 K Neutron bond lengths (Ross & Williams, 1973)	300 K X-ray	
	Uncorrected	Corrected	Uncorrected	Uncorrected	Corrected
O(1)—N(4)	1·297 (1)	1·297	1·288	1·298 (2)	1·304
O(2)—N(5)	1·236 (1)	1·237	1·222	1·224 (3)	1·233
O(3)—N(5)	1·233 (1)	1·234	1·219	1·225 (3)	1·236
N(4)—C(6)	1·368 (2)	1·370	1·366	1·360 (3)	1·372
N(4)—C(10)	1·368 (1)	1·369	1·371	1·364 (3)	1·373
N(5)—C(8)	1·454 (1)	1·455	1·458	1·453 (3)	1·460
C(6)—C(7)	1·378 (2)	1·378	1·381	1·362 (3)	1·369
C(7)—C(8)	1·387 (1)	1·388	1·388	1·380 (3)	1·389
C(8)—C(9)	1·386 (2)	1·388	1·389	1·383 (3)	1·395
C(9)—C(10)	1·375 (2)	1·376	1·378	1·353 (3)	1·359
C(6)—H(C6)	0·95 (1)		1·085	0·89 (2)	
C(7)—H(C7)	1·01 (2)		1·076	0·95 (2)	
C(9)—H(C9)	0·97 (1)		1·079	0·92 (2)	
C(10)–H(C10)	0·95 (1)		1·099	0·96 (2)	

necessity of the bond-length correction. The C–C bonds parallel to the molecular axis are slightly shorter than other C–C ring bonds, as has been generally observed in aromatic compounds with *para* substituents, indicating a contribution of quinoid resonance structures. However, the shortening (to $l=1.377$ Å) is much smaller than reported earlier [$l=1.337$ Å (Eichhorn, 1956)]. Other features are similar to those observed earlier in aromatic nitro compounds and will not be discussed further here (see, *e.g.*, Coppens & Schmidt, 1965; Holden & Dickinson, 1969). The nitroxide N–O distance [1·297 (1) at 30 K; 1·298 (2) Å at 300 K before correction for thermal shortening] is within the range of those reported earlier for pyridine *N*-oxide [X-ray diffraction $l=1.33$, 1·37 Å (Ülku, Huddle & Morrow, 1971); microwave spectroscopy $l=1.278(1)$ Å (Snerling, Nielsen, Nygaard, Pedersen & Sørensen, 1975); gas phase electron diffraction $l=1.290$ (15) Å (Chang, 1974)].

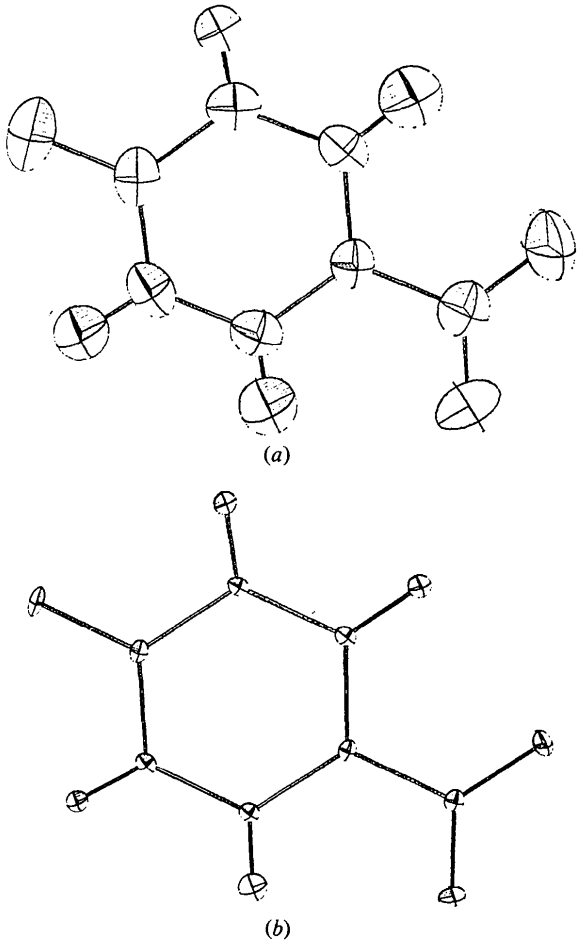

Fig. 2. 50% probability thermal ellipsoids from the X-ray refinements (*a*) at 300 K, (*b*) at 30 K. Hydrogen atoms were refined isotropically.

The neutron C–C and C–N bond lengths (Ross & Williams, 1973) agree well with X-ray values, but systematic discrepancies are observed for C–H and N–O bonds (Table 4). Both effects may be attributed to the shortcomings of the spherical-atom formalism in the least-squares X-ray refinement. An analysis of the positional parameters reveals shifts between 0·007 and 0·013 Å for the X-ray positions of N(5), O(1), O(2) and O(3), the O atoms being shifted towards the lone-pair density while the nitro-group N is displaced into the C–N bond. The size of these shifts is as observed in other studies (Coppens, 1974) and indicates the dominant effect of low-order reflections even in a refinement including a large number of high-order data. It is of interest that while the shifts are reduced in the high-order refinement ($\sin\theta/\lambda>0.75$ Å^{-1}, Table 2), systematic discrepancies persist for the four affected atoms, suggesting a persistence of valence-electron scattering beyond 0·75 Å^{-1}. This is confirmed by the electron density maps discussed below.

Thermal motion

Atomic temperature parameters (U_{ij}) from the X-ray measurements at 300 K and 30 K are listed in Table 2. Equivalent B values at 30 K are 0·5–0·8 Å^2, so that

Table 5. *Results of thermal motion analysis*

$[\sum(\Delta U_{ij})^2/(m-s)]^{1/2}$		30 K 0·0015 Å^2				300 K 0·0046 Å^2		
	Eigenvalues	Direction cosines (relative to inertial axes)			Eigenvalues	Direction cosines (relative to inertial axes)		
L (radian^2)	0·0020 (7)	0·9847	−0·1742	0·0000	0·0130 (24)	0·9786	−0·2050	0·0
	0·0006 (1)	0·0	0·0	−1·0	0·0047 (4)	0·0	0·0	−1·0
	0·0006 (1)	0·1742	0·9847	−0·0	0·0046 (4)	0·2060	0·9786	0·0
T (Å^2)	0·0057 (4)	0·9370	−0·3495	0·0	0·0358 (15)	0·9183	−0·3960	0·0
	0·0049 (6)	0·0	0·0	−1·0	0·0250 (20)	0·3960	0·9783	0·0
	0·0043 (9)	0·3493	0·9370	0·0	0·0249 (33)	0·0	0·0	1·0
S	$S_{13}=0.0001$ (1), $S_{23}=-0.0001$ (1)				$S_{13}=0.0012$ (4), $S_{23}=-0.0009$ (2)			

Transformation matrix from crystal axes to inertial axes of unit length

Low temperature			Room temperature		
8·2932	0·0	−5·8533	8·1856	0·0	−5·8804
9·3500	0·0	−5·1917	9·4866	0·0	5·1603
0·0	−5·8140	0·0	0·0	−6·010	0·0

at 30 K the soft organic crystal is being studied under conditions typical for a mineral at room temperature. The temperature parameters are typically reduced by a factor of six on cooling to 30 K, though the directions of the principal axes of the vibration tensors are generally unaffected (Fig. 2). This is also evident from the rigid-body thermal motion analysis (Table 5), which shows the main libration to be around the long axis of the molecule, while the translations are much more isotropic. The anisotropy of the librational motion is due to the moment of inertia around the long axis being 5–6 times smaller than the moments around the other two inertial axes.

It is of interest to examine how well the reduction in thermal motion agrees with a simple harmonic model represented by the expression

$$\langle u^2\rangle,\ \langle\theta^2\rangle = h[4\pi^2 Iv]^{-1}[0{\cdot}5 + \{\exp(hv/kT) - 1\}^{-1}]$$

where I is the molecular mass or the moment of inertia, and $\langle u^2\rangle$ and $\langle\theta^2\rangle$ are the mean square amplitudes in cm^2 and radians squared for translational vibrations and librations, respectively.

Plots of the frequency against mean square displacement at both 30 and 300 K are shown in Fig. 3. Within the errors of the experimental **T** and **L** values, agreement between calculated harmonic frequencies at the two temperatures is rather good. The large libration around the long axis of the molecule corresponds, for example, to frequencies of 18–24 cm^{-1} based on the 30 K results, and 21–24 cm^{-1} for the 300 K data (the range corresponds to one standard deviation of the **T** and **L** values). The only apparent discrepancy occurs for the frequency of the T_{22} translation along the normal to the molecular plane, which corresponds to $\nu = 41$–46 cm^{-1} at 300 K and $\nu = 32$–37 cm^{-1} at 30 K. This difference would be larger if the low-temperature analysis were based on the high-order U_{ij} values, since high-order U_{22} vibrational parameters tend to be larger than the full data parameters by 0–15% (Table 2). A similar effect cannot be observed at room temperature where high-order reflections are unobservable. It would, however, be less important relative to the larger U_{ij} values. Even for the T_{22} frequencies, the differences are not large considering the standard deviations, and it may be concluded that the ratio of the r.m.s. amplitudes at the two temperatures is described adequately by the harmonic model.

Valence and deformation densities

The valence density in the molecular plane, shown in Fig. 4, is obtained by subtracting Hartree–Fock core electron densities for the neutral C, N and O atoms using scattering factors given by Fukamachi (1971). Both in the valence map and in the deformation density maps discussed below, high-order ($\sin\theta/\lambda > 0{\cdot}75$ Å^{-1}) X-ray thermal parameters were used for C, N and O; all positional parameters and H thermal parameters were taken from the neutron results. Because of the use of X-ray thermal parameters the X–N maps given here are not free of bias owing to errors in the scattering model, especially in the regions around the O atoms.

The valence density shows distinct peaks at the O and N atoms while the C valence electrons are strongly smeared into the bonding regions. The valence map is qualitatively similar to those of glycylglycine (Griffin & Coppens, 1975) and uracil (Stewart, 1968).

In the deformation densities (Figs. 5 and 6) neutral spherical atoms are subtracted from the observed density. In earlier room-temperature work evidence

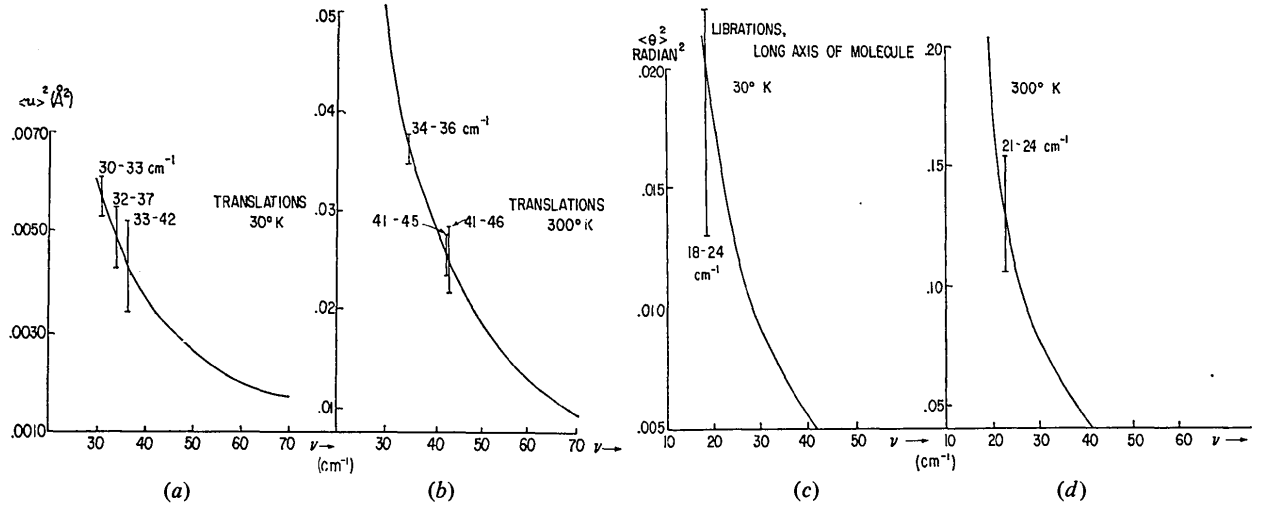

Fig. 3. Mean square amplitudes as a function of frequency according to the simple harmonic model for which the equation is given in the text; (*a*) for translational vibrations of a molecule with the mass of *p*-nitropyridine *N*-oxide at 30 K; (*b*) as (*a*) at 300 K; (*c*) for librational motion around the long axis of the molecule at 30 K; (*d*) as (*c*) at 300 K. Vertical bars indicate experimental **T** and **L** values within one standard deviation.

was obtained for the persistence of the lone-pair scattering into the high-order region (Becker, Coppens & Ross, 1973). It is therefore of interest to examine the effect on the lone-pair peak heights in the present study in which an unusually large number of high-order reflections are available.

The three deformation density maps with maximum $\sin\theta/\lambda$ values of 0·65, 0·75, and 1·0 Å^{-1} (full data) are shown in Fig. 5. As the scale factor was practically independent of the data cut-off in the X-ray refinement, the full data value was used in all maps. It is evident that the height of the lone-pair features on the O atoms increases with data cut-off, the lone-pair peaks in the full-data Fourier map being almost twice as high as in the low-angle function. The change in the bond density is much less pronounced, as would be expected on the basis of considerations given earlier (Becker, Coppens & Ross, 1973; Coppens, 1969). Unfortunately, the full data maps have an unusually high noise level in areas away from the bonding and lone-pair regions. To examine if this might result from the inclusion of a large number of weak high-order reflections, the summation was repeated using only reflections with $F>6\sigma(F)$. As this second map is quite similar to the one shown in Fig. 5, the noisy appearance is probably due to the relative lack of precision in the high-order data. More information on this effect can be obtained when reliable neutron thermal parameters become available.

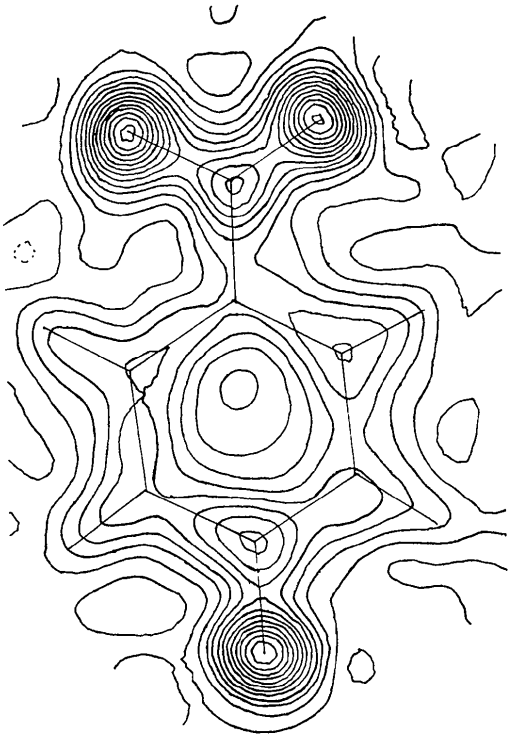

Fig. 4. Valence density in the plane of the molecule (at 30 K). Contours at 0·5 e Å^{-3}, negative contours dotted. The density at the center of the ring is slightly negative.

Further features to be noted are the low values of peak heights in the terminal N–O bonds (attributed to the use of high-order X-ray rather than neutron thermal parameters) and the differences in C–C bond peak heights in the aromatic ring, which are larger in the bonds adjacent to the nitro group. A section perpendicular to the ring bonds which are parallel to the molecule's long axis shows an extension perpendicular to the molecular plane indicative of π-character of the bonds. A comparable but less pronounced effect is apparent in the other cyclic C–C bonds. Similar observations have been made in a number of other compounds [*e.g.*, *sym*-triazine (Coppens, 1967); tetracyanoethylene (Becker, Coppens & Ross, 1973), and a series of hydrocarbons (Irngartinger, Leiserowitz & Schmidt, 1970)].

Finally, the X–X map based entirely on high-order X-ray parameters for C, N, O and on neutron parameters for H, and including all data with $\sin\theta/\lambda>0·75$

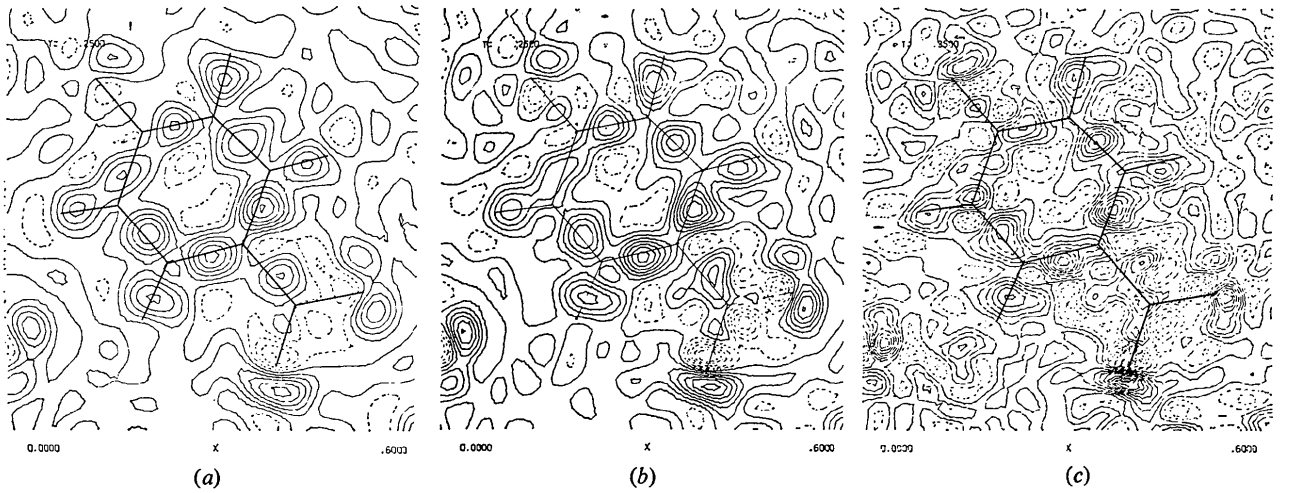

(*a*) (*b*) (*c*)

Fig. 5. X–N maps (at 30 K) obtained with high-order X-ray thermal parameters for C, N and O. Data cut-off of (*a*) 0·65 Å^{-1}, (*b*) 0·75 Å^{-1}, (*c*) full data. Contour interval 0·1 e Å^{-3}, negative contours dotted.

$Å^{-1}$ is shown in Fig. 6. This map differs from the X–N map, Fig. 5(*b*), mainly in the lone-pair and terminal bond regions. The differences are due to the asphericity shifts discussed earlier which represent significant discrepancies between X-ray and neutron positional parameters. The implication is that, even with a high-order X-ray refinement with data of $\sin\theta/\lambda > 0{\cdot}75$ $Å^{-1}$, no reliable estimate of the lone-pair density can be obtained. The situation is much more favorable for the bond regions were X-ray measurements appear adequate, provided hydrogen parameters can be deduced from other information.

Conclusions

The comparison of the difference density maps strongly suggests that high-order refinements with data at $\sin\theta/\lambda = 0{\cdot}65$–$1{\cdot}0$ $Å^{-1}$ or $0{\cdot}75$–$1{\cdot}0$ $Å^{-1}$ do not lead to completely unbiased estimates of the atomic positional and thermal parameters. Additional studies, possibly with Ag $K\alpha$ radiation, are needed to investigate refinements with data beyond 1 $Å^{-1}$. The weakness of the X-ray scattering in this region, even at low temperatures, raises experimental problems which need further investigation. Thus, the present X–X difference densities are not a satisfactory substitute for X–N densities obtained by a combination of X-ray and neutron diffraction, especially in the regions of the lone pair electrons. However, X-ray data appear sufficient for a qualitative study of the density in the bonds between atoms.

Support of this work by the National Science Foundation is gratefully acknowledged. We are grateful to Dr William F. Cooper for his help during the liquid-helium data collection experiment.

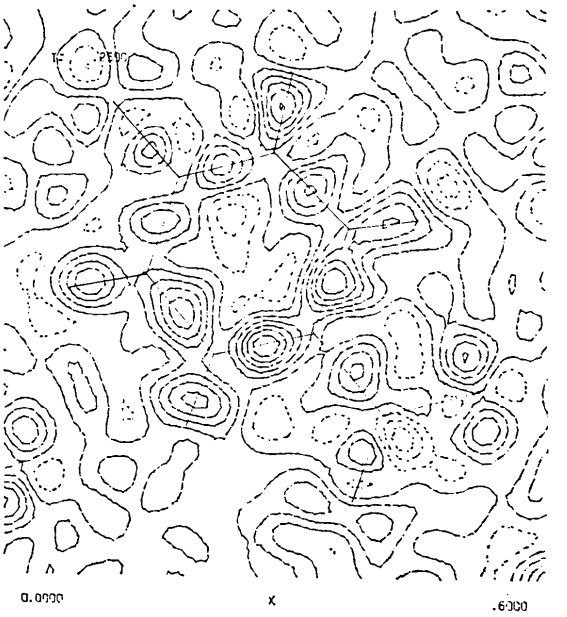

Fig. 6. X–X maps (at 30 K) using neutron parameters for the hydrogen atoms. Data cut-off $0{\cdot}75$ $Å^{-1}$. Contours as in Fig. 5.

References

BECKER, P., COPPENS, P. & ROSS, F. K. (1973). *J. Amer. Chem. Soc.* **95**, 7604–7609.

BLESSING, R. H., COPPENS, P. & BECKER, P. (1974). *J. Appl. Cryst.* **7**, 488–492.

CHANG, J. F. (1974). *J. Chem. Phys.* **61**, 1280–1283.

COPPENS, P. (1967). *Science*, **158**, 1577–1579.

COPPENS, P. (1969). *Acta Cryst.* A**25**, 180–186.

COPPENS, P. (1974). *Acta Cryst.* B**30**, 255–261.

COPPENS, P. (1975). *MTP International Review of Science: Physical Chemistry*. Series 2, Vol. II, edited by J. M. ROBERTSON. London: Butterworths.

COPPENS, P., ROSS, F. K., BLESSING, R. H., COOPER, W. F., LARSEN, F. K., LEIPOLDT, J. G., REES, B. & LEONARD, R. (1974). *J. Appl. Cryst.* **7**, 315–322.

COPPENS, P. & SCHMIDT, G. M. J. (1965). *Acta Cryst.* **18**, 654–663.

COPPENS, P. & VOS, A. (1971). *Acta Cryst.* B**27**, 146–158.

COULSON, C. A. & THOMAS, M. W. (1971). *Acta Cryst.* B**27**, 1354–1359.

EICHHORN, E. L. (1956). *Acta Cryst.* **9**, 787–793.

FUKAMACHI, T. (1971). Tech. Rep. Inst. Solid State Phys. B**12**, Univ. of Tokyo, Japan.

GRIFFIN, J. F. & COPPENS, P. (1975). *J. Amer. Chem. Soc.* **97**, 3496–3505.

HOLDEN, J. R. & DICKINSON, C. (1969). *J. Phys. Chem.* **73**, 1199–1204.

International Tables for X-ray Crystallography (1974). Vol. IV. Birmingham: Kynoch Press.

IRNGARTINGER, H., LEISEROWITZ, L. & SCHMIDT, G. M. J. (1970). *J. Chem. Soc.* (*B*), pp. 497–504.

ROSS, F. K. & WILLIAMS, J. M. (1973). Private communication.

RUYSINK, A. F. J. & VOS, A. (1974). *Acta Cryst.* A**30**, 497–503.

SCHOMAKER, V. & TRUEBLOOD, K. N. (1968). *Acta Cryst.* B**24**, 63–76.

SNERLING, O., NIELSEN, C. J., NYGAARD, L., PEDERSEN, E. J. & SØRENSEN, G. O. (1975). *J. Mol. Struct.* **27**, 205–211.

STEWART, R. F. (1968). *J. Chem. Phys.* **48**, 4882–4889.

STEWART, R. F., DAVIDSON, E. R. & SIMPSON, W. T. (1965). *J. Chem. Phys.* **42**, 3175–3187.

ÜLKÜ, D., HUDDLE, B. P. & MORROW, J. C. (1971). *Acta Cryst.* B**27**, 432–436.

VERSCHOOR, G. C. & KEULEN, E. (1971). *Acta Cryst.* B**27**, 134–145.